Model Predictive Direct Power Control for Grid-Connected Converters

Tobias Geyer, James Scoltock and Udaya Madawala
Department of Electrical and Computer Engineering
The University of Auckland
1052 Auckland, New Zealand
Email: t.geyer@ieee.org, jsco075@aucklanduni.ac.nz, u.madawala@auckland.ac.nz

***Abstract*—This paper presents a Model Predictive Direct Power Control (MPDPC) scheme for the control of three-phase grid-connected Voltage Source Converters (VSCs). MPDPC builds on the well-known Direct Power Control (DPC) scheme by utilising a state-space model of the system to predict the future behaviour of the system. MPDPC achieves optimal performance by minimising the switching losses or switching frequency of the converter while regulating the output real and reactive powers. The scheme presented here utilises the Virtual Flux (VF) estimation technique which enables accurate estimation of the output real and reactive power without the use of line-voltage sensors. Through simulation, it is shown that at a fixed level of current distortion, MPDPC is capable of outperforming Pulse Width Modulation (PWM) in terms of switching losses.**

***Index Terms*—Model predictive control, direct power control, grid connected converter**

I. Introduction

In recent years there has been a surge in the number of Voltage Source Converters (VSCs) connected to the electrical grid. Such converters are popular in the grid integration of renewable energy systems such as wind turbines and photovoltaic cells [1]. Grid connected VSCs are also beginning to be used in transmission and distribution networks in such applications as Static Synchronous Compensators (STATCOM) and High Voltage Direct Current (HVDC) transmission systems [2], [3]. Additionally, grid-connected VSCs are used in a variety of industrial applications, such as in motor drive front ends [4]. As such, reliable and efficient control and modulation schemes are essential for grid-connected VSCs.

Model Predictive Control (MPC), which was developed in the process control industry in the 1970's [5], has received significant attention from industry and academia. However, MPC has only recently been applied to power electronics. Model Predictive Direct Torque Control (MPDTC), which was initially developed in 2003 [6] - [8], is a variant of MPC which builds on the well known Direct Torque Control (DTC) technique. MPDTC utilises the hysteresis bounds of DTC, but removes the switching table which is used in DTC to select converter states, replacing it with an online-optimisation stage. Successful test runs for MPDTC have been carried out on the ABB ACS 6000 drive with power levels in excess of 1 MW [9].

Direct Power Control (DPC) is a popular scheme for the control of grid-connected converters. DPC directly controls the real and reactive power of the converter by selecting the switching state of the converter [10], [11]. DPC selects an optimal converter state in a similar manner to DTC by utilising a switching table and hysteresis bounds. In [12], the Virtual Flux (VF) technique was first proposed for DPC. The VF technique makes the assumption that the grid voltage and AC-side resistance and inductance are quantities which can be related to an AC machine [13]. The use of VF vectors in DPC enables the elimination of grid voltage sensors and a simple power calculation.

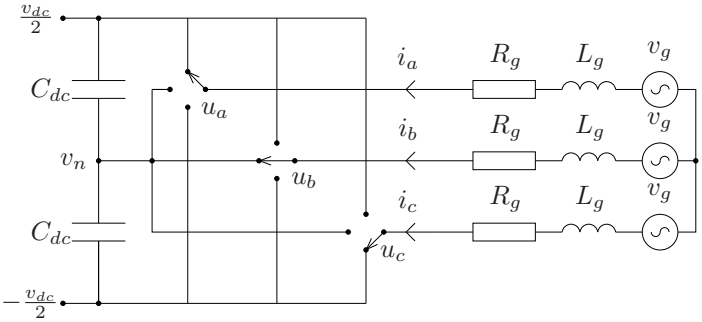

Fig. 1: Representation of a three-level, three-phase NPC converter connected to the grid

In the same way that MPDTC extends on DTC, Model Predictive Direct Power Control (MPDPC) can be viewed as an extension of DPC, replacing the switching table with an online-optimisation stage. This paper presents a VF-based MPDPC scheme for three-phase grid-connected VSCs. Under steady-state conditions, the key performance indicators are the converter switching losses, P_{sw}, and the Total Demand Distortion (TDD) of the grid current, I_{TDD}. Under transient conditions performance is judged by the response time of the output following reference steps. In order to benchmark the performance of MPDPC, it has been compared against Pulse Width Modulation (PWM) and Optimised Pulse Patterns (OPP). The different schemes have been compared through simulation of a three-level, three-phase Neutral Point Clamped (NPC) converter.

II. Grid Connected Converter System

A. System Setup

A representation of a three-level, three-phase grid-connected NPC converter is shown in Fig. 1. The DC-link is assumed to be feeding a load such as an MV motor drive. It should be noted that a step-down transformer is used in connecting the converter to the grid; the voltage is stepped down from 33 kV to 3 kV, with the leakage inductance of the transformer included in the grid inductance parameter L_g. All values are referred to the low-voltage (converter side) of the transformer.

B. $\alpha\beta$ Reference Frame

Variables $\xi_{abc} = [\xi_a\ \xi_b\ \xi_c]^T$ in the three-phase abc reference frame are transformed to $\xi_{\alpha\beta} = [\xi_\alpha\ \xi_\beta]^T$ in the orthogonal $\alpha\beta$ reference frame through

$$\xi_{\alpha\beta} = \frac{2}{3} P \xi_{abc} \tag{1}$$

where P is the transformation matrix

$$P = \begin{bmatrix} 1 & -\frac{1}{2} & -\frac{1}{2} \\ 0 & \frac{\sqrt{3}}{2} & -\frac{\sqrt{3}}{2} \end{bmatrix}. \tag{2}$$

C. Inverter Model

Each phase leg of the converter is able to assume one of three states, which can be represented by the integer variables $u_a, u_b, u_c \in \{-1, 0, 1\}$. Since there are three switching states per phase and three phases, there are $3^3 = 27$ possible switching states of the form $u_{abc} = [u_a\ u_b\ u_c]^T$. Within those states there are 19 distinct voltage vectors which the inverter is capable of producing. The voltage vectors can be represented by transforming the switching states to the orthogonal $\alpha\beta$ system, yielding vectors of the form $u_{\alpha\beta} = [u_\alpha\ u_\beta]^T$. The voltages as they appear across the output of the converter are given by

$$v_c = \frac{v_{dc}}{2} u_{\alpha\beta} \tag{3}$$

where $v_c = [v_{c\alpha}\ v_{c\beta}]^T$. In the converter considered all switching transitions are allowed except for those which involve switching between the upper and lower rails. For example, a transition from u_{abc} = [1 1 1]^T to [0 0 1]^T is allowed, whereas a transition to [-1 1 1]^T is not.

The neutral point potential, v_n, depends on the state of the converter and therefore the voltage across each of the DC-link capacitors. It is only affected when current is directly drawn from it when one or more of the switching states is zero. From [8] it follows that

$$\frac{dv_n}{dt} = -\frac{1}{2C_{dc}}((1-|u_a|)i_a + (1-|u_b|)i_b + (1-|u_c|)i_c) \tag{4}$$

where C_{dc} is the value of each of the two capacitors of the DC-link and i_a, i_b, i_c are the grid phase currents. Since it is assumed that $i_a + i_b + i_c = 0$, it follows that

$$\frac{dv_n}{dt} = \frac{1}{2C_{dc}} |u_{abc}|^T i_{abc} \tag{5}$$

where $|u_{abc}| = [|u_a|\ |u_b|\ |u_c|]^T$ and $i_{abc} = [i_a\ i_b\ i_c]^T$.

D. Grid Model

The addition of the VF strategy to DPC enables the estimation of real and reactive power without measurement of the grid voltage. The VF technique draws analogy between the grid voltage, v_g and line parameters, R_g and L_g, and an AC machine. R_g and L_g represent the stator resistance and leakage inductance of the AC machine, respectively, while v_g represents the back EMF of the machine. Fig. 2 illustrates the VF-based grid model. The grid voltage can be estimated from the measured grid current i and converter voltage v_c

$$v_g = v_c + R_g i + L_g \frac{di}{dt} \tag{6}$$

where $v_g = [v_{g\alpha}\ v_{g\beta}]^T$ and $i = [i_\alpha\ i_\beta]^T$. The VF of the grid and converter are subsequently defined as

$$\Phi_g = \int v_g dt \tag{7}$$

$$\Phi_c = \int (v_c + R_g i) dt \tag{8}$$

where $\Phi_g = [\Phi_{g\alpha}\ \Phi_{g\beta}]^T$ and $\Phi_c = [\Phi_{c\alpha}\ \Phi_{c\beta}]^T$. The grid current i can subsequently be expressed in terms of the grid and converter VF as

$$i = \frac{1}{L_g}(\Phi_g - \Phi_c). \tag{9}$$

As defined in [14], the instantaneous real and reactive grid powers are given by

$$p = \frac{3}{2}(v_{g\alpha} i_\alpha + v_{g\beta} i_\beta) \tag{10}$$

$$q = \frac{3}{2}(v_{g\alpha} i_\beta - v_{g\beta} i_\alpha) \tag{11}$$

From (7), (10) and (11), the instantaneous real and reactive powers can be expressed in terms of the grid current and VF as

$$p = \frac{3\omega}{2}(\Phi_{g\alpha} i_\beta - \Phi_{g\beta} i_\alpha) \tag{12}$$

$$q = -\frac{3\omega}{2}(\Phi_{g\alpha} i_\alpha + \Phi_{g\beta} i_\beta) \tag{13}$$

where ω is the angular frequency of the grid.

III. Internal Model of the Controller

A discrete-time model of the system is required to serve as an internal prediction model for the controller. The model is used by the controller to predict the trajectory of the real and reactive power and converter neutral point potential over a succession of sampling intervals, and is derived under the assumption that the direction of power flow is from grid to converter. The state vector of the system is defined as

$$x = [i_\alpha\ i_\beta\ \Phi_{g\alpha}\ \Phi_{g\beta}\ v_n]^T \tag{14}$$

the input vector is defined as the converter switch positions

$$u = [u_a\ u_b\ u_c]^T \in \{-1, 0, 1\}^3 \tag{15}$$

and the output vector is defined as the instantaneous real and reactive power and converter neutral point potential

$$y = [p\ q\ v_n]^T. \tag{16}$$

A discrete-time model of the system can subsequently be expressed as

$$\begin{aligned} x(k+1) &= (I + AT_s)x(k) + B_1 T_s u(k) \\ &\quad + \begin{bmatrix} 0^T & B_2^T(x(k)) \end{bmatrix}^T T_s |u(k)| \end{aligned} \tag{17}$$

$$y(k) = g(x(k)) \tag{18}$$

where A is the state matrix

$$A = \begin{bmatrix} -\frac{R_g}{L_g} & 0 & 0 & -\frac{\omega}{L_g} & 0 \\ 0 & -\frac{R_g}{L_g} & \frac{\omega}{L_g} & 0 & 0 \\ 0 & 0 & 0 & -\omega & 0 \\ 0 & 0 & \omega & 0 & 0 \\ 0 & 0 & 0 & 0 & 0 \end{bmatrix} \tag{19}$$

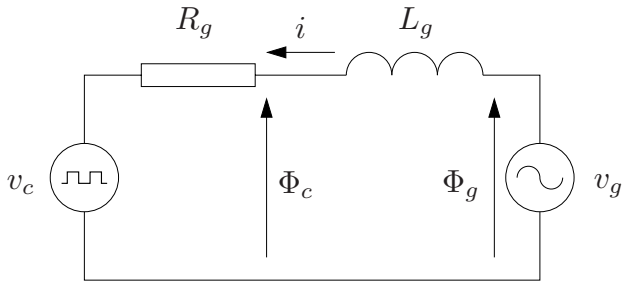

Fig. 2: Single-phase diagram showing the definition of the virtual-flux vectors

B_1 and $B_2(x(k))$ are the input matrices

$$B_1 = -\frac{v_{dc}}{3L_g}\begin{bmatrix} P^T & 0 \end{bmatrix}^T \tag{20}$$

$$B_2(x(k)) = \frac{3}{4C_{dc}}(x(k))^T\begin{bmatrix} P^{-1} & 0 \end{bmatrix}^T \tag{21}$$

and $g(x(k))$ is the output function

$$g(x(k)) = \begin{bmatrix} \frac{3\omega}{2}(x_2(k)x_3(k) - x_1(k)x_4(k)) \\ -\frac{3\omega}{2}(x_1(k)x_3(k) + x_2(k)x_4(k)) \\ x_5(k) \end{bmatrix}. \tag{22}$$

In this model, I is the 5x5 identity matrix and T_s is the sampling interval of $25\mu s$. The zeros in (17), (20) and (21) are vectors and matrices of appropriate dimensions.

IV. Model Predictive Direct Power Control

Fig. 3 illustrates the MPDPC control scheme for the grid-connected converter system under consideration. MPDPC forms the inner control loop and is directly responsible for setting the switching states of the converter. The outer control loop is a PI controller which regulates the value of the power reference p^* based on the total DC-link voltage v_{dc}. The fundamental control objective of MPDPC is to keep the instantaneous value of the real and reactive powers, p and q, within a set of symmetrical hysteresis bounds around the reference values p^* and q^*. δ_P denotes the difference between the upper (or lower) real power bound and p^*, while δ_Q has the same meaning for reactive power. In addition, the controller must ensure that the neutral point potential v_n stays within a hysteresis bound about zero. The width of the hysteresis bounds directly determines the level of harmonic distortion which will be present in the output signals, and therefore sets the trade-off between current distortion and switching frequency. At each time-step k the state variables are determined, and by predicting the future trajectory of the real and reactive power for each feasible future switching sequence, an optimal switching state which minimises the switching frequency or switching losses is calculated via a cost function.

A. Switching and Prediction Horizons

In describing MPDPC it is important to distinguish between the switching horizon N_s and prediction horizon N_p. The switching horizon refers to the number of switching transitions within a prediction, with extension of the power trajectory occuring after each switching event until one or more hysteresis bounds are hit, at which point another switching event may take place. As such, the switching horizon can be defined in terms of the elements 'S' and 'E', for switch and extend respectively. A switching horizon of 'eSESE' is therefore composed of a switching transition, an extension until one or more bounds are hit, a second switching transition, and a second extension until one or more bounds are hit. Note that the lower case 'e' refers to an optional extension leg at the beginning of the switching horizon. The prediction horizon N_p refers to the total number of time-steps into the future for which the prediction is made, which will vary based on the exact switching sequence which is being predicted.

B. Control Procedure

During the control procedure, it is important to identify candidate sequences. A candidate sequence is one for which both the p and q components and the neutral point potential v_n are either within the hysteresis bounds or 'pointing' in the direction of the bounds (outside the bounds but moving closer to them) at every time-step of the prediction [8]. At each time-step k, the state variables $x(k)$ are determined and from those values the output variables $p(k)$ and $q(k)$ are calculated. Given the previous switch position $u(k-1)$, the hysteresis bounds and the internal prediction model, the controller computes at time instant k the three-phase switch position $u(k)$ to be applied based on the following procedure (assuming a switching horizon of 'SESE'):

1) Given $u(k-1)$, determine the allowable switching sequences over the switching horizon N_s, with $i \in \mathcal{I}$ for each switching sequence U^i.
2) For each allowable sequence, simulate the first 'S' event at time-instant k. Predict the trajectory of p, q and v_n at time-instant $k+1$ using the internal prediction model. Using either the internal prediction model or an extrapolation technique, extend the trajectories until one or more bounds are violated. Disregard those sequences which are not candidates. For each candidate switching sequence U^i with $i \in \mathcal{I}_a \subseteq \mathcal{I}$, the number of time steps taken from time-step k until the bound(s) is violated during the first extension is denoted as N^i_{p1}.
3) Simulate the second 'S' event at $k + N^i_{p1}$ for each remaining sequence. Predict the trajectory of p, q and v_n in the same way as outlined in Step 2. For each remaining candidate sequence U^i with $i \in \mathcal{I}_b \subseteq \mathcal{I}_a$, the number of time steps taken from time-step $k+N^i_{p1}$ until the bound(s) is violated during the second extension is denoted as N^i_{p2}.
4) For each candidate switching sequence U^i, calculate the length of the prediction horizon $N^i_p = N^i_{p1} + N^i_{p2}$ where $i \in \mathcal{I}_b$.
5) For each candidate switching sequence U^i compute the cost

$$C^i = \frac{1}{N^i_p}\sum_{\ell=k}^{k+N^i_p} \|u^i(\ell) - u^i(\ell-1)\|_1 \tag{23}$$

for minimisation of switching frequency, or

$$C^i = \frac{E^i}{N^i_p} \tag{24}$$

for minimisation of switching losses. Here E^i is the total switching energy loss over the prediction horizon.

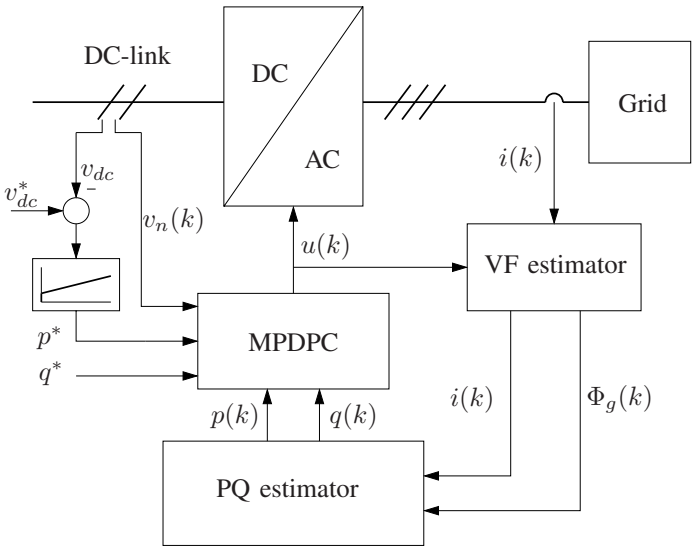

Fig. 3: MPDPC for a grid-connected NPC converter

A detailed description of the calculation of switching losses is given in [8].

6) Choose the switching sequence with the minimal cost

$$i = \arg\min_{i \in \mathcal{I}_b} C^i \tag{25}$$

7) Apply the switch position $u(k) = U^i(k)$ and shift the horizon one step forward.

At the next sampling instant the above process is repeated and a new switch position is calculated at $k+1$. It should be noted that when p, q and v_n are within their bounds at the sampling instant k, it may be the case that the optimal switching sequence will involve reapplying the switch position $u(k-1)$ at $u(k)$.

Fig. 4 shows a hypothetical set of predicted output trajectories over a switching horizon of 'SESE' for a pair of candidate switching sequences. At time-step k switching is necessitated due to violation of the lower real power bound p_{min} with $u(k-1) = \{0,0,0\}$. At this point the first 'S' event occurs, with sequences 1 and 2 transitioning to the states $u = \{1,1,0\}$ and $\{0,-1,0\}$ respectively. Following the first extension event 'E' for each sequence, the second switching event results in sequences 1 and 2 branching to $u = \{1,0,1\}$ and $\{0,-1,1\}$ respectively, with both switching events again extended until bound violation occurs. For each sequence, the solid lines represent the trajectory of the switching event, while the dashed lines represent their extensions. The solid circles represent switching events, while the hollow circles represent the beginning of extensions.

From Table I it is clear that sequence 2 has a lower cost (for switching frequency minimisation) than sequence 1. If $u(k)$ had to be selected from these sequences, then the optimal solution would be to apply the vector $u(k) = \{0,-1,0\}$ to the converter.

TABLE I: Summary of the switching sequences of Fig 4.

Sequence number i	Sequence length N_p^i	Number of switch transitions S^i	Cost C^i
1	6	4	2/3
2	7	2	2/7

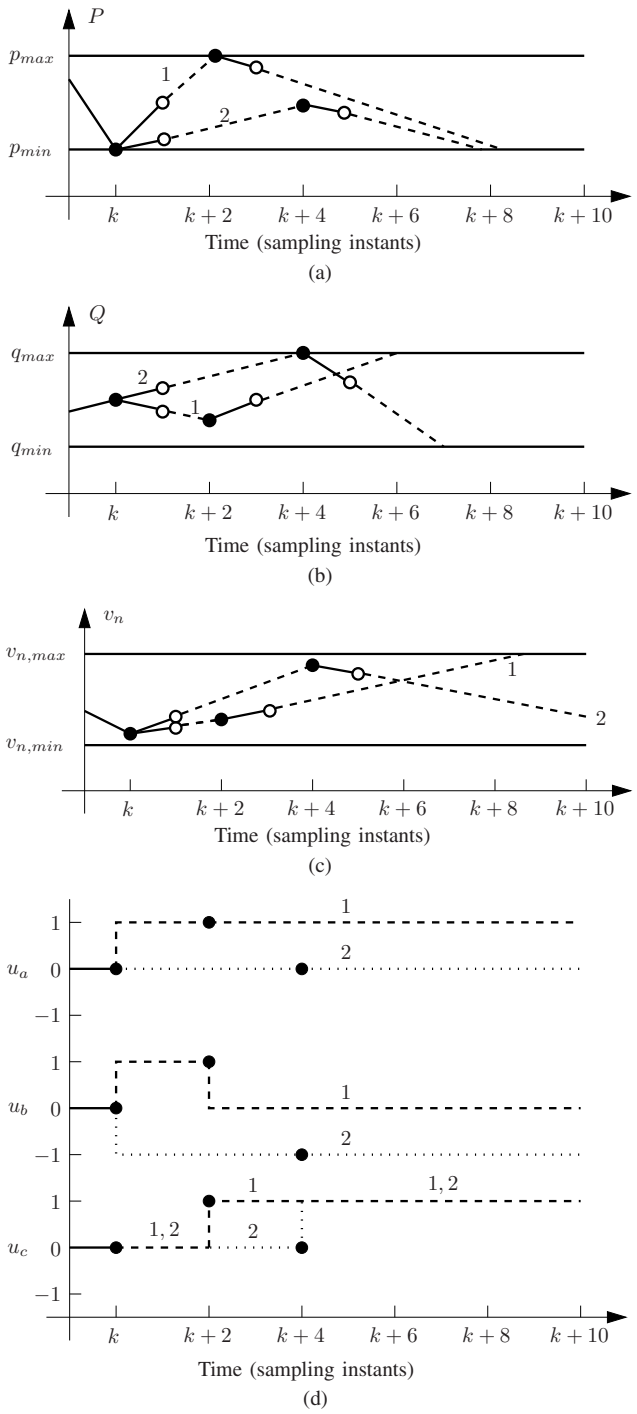

Fig. 4: Predicted real power (a), reactive power (b) and neutral point potential (c) trajectories for the switching sequences of (d). The numbers on all diagrams refer to the indices of the switching sequences.

V. Performance Evaluation

This section summarizes the simulation results for MPDPC using the grid-connected converter system as described in Section II. A standard three-level, three-phase NPC converter has been used. The semiconductors used are the ABB 35L4510 4.5 kV 4 kA Integrated Gate Commutated Thyristor (IGCT) and the ABB 10H4520 fast recovery diode. A summary of the nominal grid and converter parameters is shown in Table II.

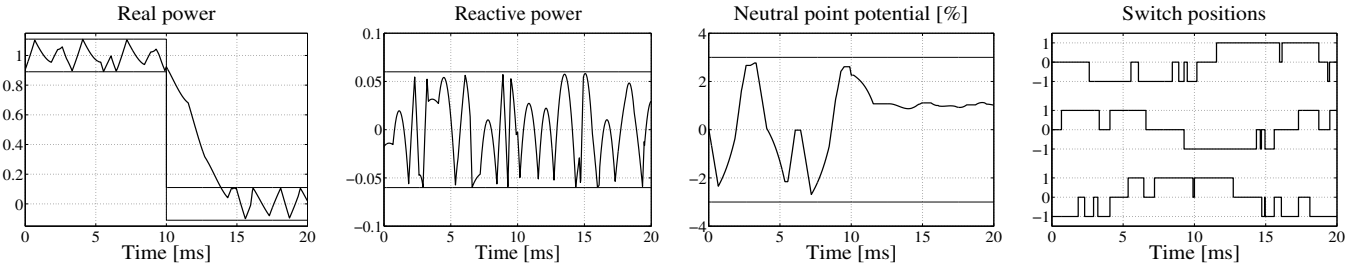

Fig. 5: MPDPC with a switching horizon of 'eSESE', real power bound width of $\delta_P = 0.11$ p.u and reactive power bound width of $\delta_Q = 0.06$ p.u. At $t = 10$ ms there is a power step from 1 to 0 p.u. The real and reactive power, neutral point potential and switch sequences are plotted over one fundamental period.

TABLE II: Rated values (left) and parameters (right) of the system

Grid			
Voltage	3000 V	R_g	0.0890 p.u.
Current	1540 A	L_g	0.5585 p.u.
Frequency	50 Hz		
Inverter			
DC-link voltage	5200 V	C_{dc}	3.5343 p.u.
Apparant power	8 MVA		

The per unit (p.u.) system, which is used in all simulations, is developed from foundation values of $V_{base} = \sqrt{2/3}V_g$ = 2449 V, P_{base} = 8 MVA and f_{base} = 50 Hz.

In order to benchmark the performance of MPDPC, the results are compared against those of the PWM and Optimised Pulse Pattern schemes. PWM is well-established in the control of grid-connected three-phase converters [15], [16] and as such the performance of such a scheme is a useful benchmarking tool. OPPs, which are calculated off-line, minimize the current distortion for a given pulse number (switching frequency) through optimisation of the switching angles for all possible operating points over a quarter of a fundamental period. OPPs have been used for benchmarking in previous papers on MPC in [17] and [18]. In steady state, the performance of PWM and OPP are compared against MPDPC with various switching horizons. For transient analysis, the 'eSESE' horizon for MPDPC is considered. Both PWM and OPP have been simulated with open loop V/f control.

For MPDPC the width of the hysteresis bound around the neutral point is $\pm$0.03 pu. In all simulations it is assumed that the total DC-link voltage is fixed, rendering the outer control loop described in Section IV redundant. Extension steps for MPDPC are carried out using the internal model of the controller rather than through linear or quadratic extrapolation. All MPDPC simulations have been carried out with the cost function penalising switching losses, P_{sw}.

A. Transient Performance

As shown in Fig. 5 MPDPC achieves a fast transient response to a step change in the real power reference. A step change in the real power from 1 to 0 p.u. occurs at t = 10 ms, with the controller limiting the length of the transient to about 4 ms. It should be noted that during the transient periods all other variables are kept inside their respective bounds, and rapid switching is avoided, as shown in Fig. 5d. Similarly rapid transient responses have been observed for MPC-based controllers in [8] and [18].

B. Steady-State Performance

Table III compares the performance of MPDPC with PWM and OPP in terms of current distortion I_{TDD}, switching losses P_{sw} and switching frequency f_{sw}, with all simulations run at output real power of 1 p.u. The comparison is made with a similar current distortion of about 5% for all schemes.

It is clear that extending the switching horizon, and therefore prediction horizon, significantly improves the performance of MPDPC. By extending the switching horizon, the controller is able to make better decisions as it is able to look further into the future. MPDPC with a short horizon results in switching losses 4% higher than PWM. However, by extending the switching horizon of MPDPC to 'eSESE' and 'eSESESE', the respective switching losses are 9% and 12.8% lower than PWM. Despite improving on PWM, under these conditions MPDPC falls short of OPP. With a long switching horizon, MPDPC yields switching losses significantly higher than OPP. However, the transient performance of control schemes based on OPP is usually very slow, with MPDPC having an advantage in this regard.

Figs. 6 and 7 show the output real and reactive power, neutral point potential and switch positions for PWM and MPDPC with a switching horizon of 'eSESESE' at a current distortion of about 5%. Figs. 6a - b and 7a - b show that with similar current TDD, PWM produces more ripple in the reactive output power, while MPDPC produces more ripple in the real output power.

VI. Conclusion

This paper has presented a VF-based MPDPC scheme for the control of grid-connected VSCs. A model of the grid-connected converter was derived for the controller, and an algorithm for the MPDPC procedure was described. At the chosen operating point shown in Table III, it has been shown that by increasing the switching horizon of MPDPC, the performance can be significantly improved. With a long horizon, the switching losses of MPDPC are 12.8% lower than for PWM. In this paper a three-level, three-phase NPC converter was used as this is a common example of a multi-level grid-connected VSC. MPDPC could easily be extended to other topologies and/or applications by changing the internal model of the controller.

TABLE III: Comparison of MPDPC with PWM and OPP. f_c denotes the carrier frequency for PWM and d the pulse number for OPP. The second section shows absolute values while the third section shows percentage values relative to PWM.

Control scheme	Control setting	Switching horizon	Average prediction horizon	I_{TDD} [%]	P_{sw} [kW]	f_{sw} [Hz]	I_{TDD} [%]	P_{sw} [%]	f_{sw} [%]
PWM	f_c = 450 Hz	-	-	5.147	16.60	250	100	100	100
MPDPC	δ_P = 0.080, δ_Q = 0.052	eSE	18	5.161	17.29	254	100	104	102
MPDPC	δ_P = 0.080, δ_Q = 0.048	eSESE	39	5.128	15.11	230	99.6	91.0	92
MPDPC	δ_P = 0.080, δ_Q = 0.054	eSESESE	61	5.145	14.47	233	100	87.2	93.2
OPP	d = 3	-	-	5.445	8.59	150	106	51.8	60.0

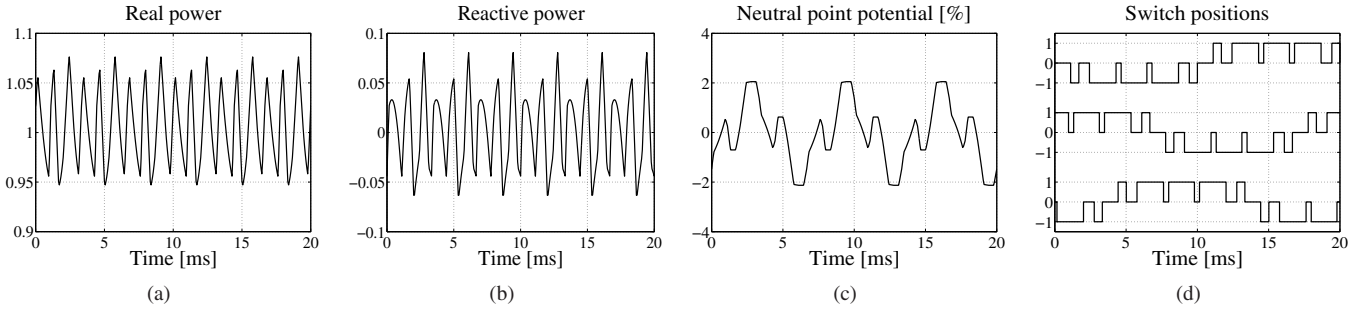

Fig. 6: PWM with a carrier frequency f_c =450 Hz.

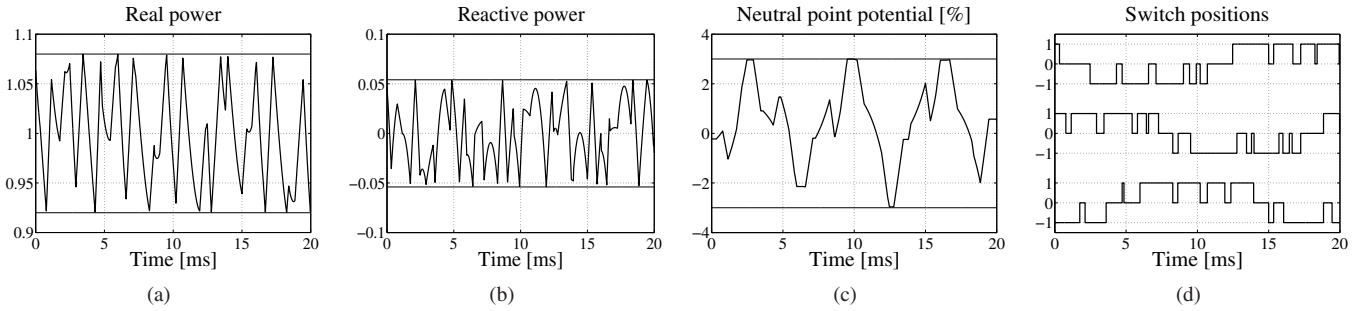

Fig. 7: MPDPC with a switching horizon of 'eSESESE' and real and reactive power hysteresis bounds of δ_P =0.080 and δ_Q =0.054.

REFERENCES

[1] F. Blaabjerg, R. Teodorescu, M. Liserre, and A.V. Timbus. Overview of control and grid synchronization for distributed power generation systems. *IEEE Trans. Ind. Electron.*, 53(5):1398 –1409, Oct. 2006.

[2] B. Singh, R. Saha, A. Chandra, and K. Al-Haddad. Static synchronous compensators (STATCOM): a review. *IET Power Electronics*, 2(4):297–324, Jul. 2009.

[3] N. Flourentzou, V.G. Agelidis, and G.D. Demetriades. VSC-based HVDC power transmission systems: An overview. *IEEE Trans. Power Electron.*, 24(3):592–602, Mar. 2009.

[4] J. Rodriguez, J.S. Lai, and F.Z. Peng. Multilevel inverters: a survey of topologies, controls, and applications. *IEEE Trans. Ind. Electron.*, 49(4):724 – 738, Aug. 2002.

[5] D. Q. Mayne, J. B. Rawlings, C. V. Rao, and P. O. M. Scokaert. Constrained model predictive control: Stability and optimality. *Automatica*, 36(6):789–814, Jun. 2000.

[6] T. Geyer. *Low Complexity Model Predictive Control in Power Electronics and Power Systems*. PhD thesis, Automatic Control Laboratory ETH Zurich, 2005.

[7] T. Geyer, G. Papafotiou, and M. Morari. Model predictive direct torque control - part I: Concept, algorithm and analysis. *IEEE Trans. Ind. Electron.*, 56(6):1894–1905, Jun. 2009.

[8] T. Geyer. Generalized model predictive direct torque control: Long prediction horizons and minimization of switching losses. In *Proc. IEEE Conf. on Decis. and Control*, Shanghai, China, Dec. 2009.

[9] G. Papafotiou, J. Kley, K.G. Papadopoulos, P. Bohren, and M. Morari. Model predictive direct torque control - part II: Implementation and experimental evaluation. *IEEE Trans. Ind. Electron.*, 56(6):1906–1915, Jun. 2009.

[10] T. Noguchi, H. Tomiki, S. Kondo, and I. Takahashi. Direct power control of PWM converter without power-source voltage sensors. *IEEE Trans. Ind. Applicat.*, 34(3):473 –479, May/Jun. 1998.

[11] D. Zhi, L. Xu, and B.W. Williams. Improved direct power control of grid-connected DC/AC converters. *IEEE Trans. Power Electron.*, 24(5):1280 –1292, May 2009.

[12] M. Malinowski, M.P. Kazmierkowski, and A. Trzynadlowski. Direct power control with virtual flux estimation for three-phase PWM rectifiers. In *Proc. IEEE Int. Symp. on Ind. Electron.*, Puebla, Mexico, Dec. 2000.

[13] M. Malinowski, M.P. Kazmierkowski, S. Hansen, F. Blaabjerg, and G.D. Marques. Virtual-flux-based direct power control of three-phase PWM rectifiers. *IEEE Trans. Ind. Applicat.*, 37(4):1019–1027, Jul./Aug. 2001.

[14] H. Akagi and A. Nabae. The *p-q* theory in three-phase systems under nonsinusoidal conditions. *Eur. Trans. Elect. Power, ETEP*, 3(1):27–31, Jan./Feb. 1993.

[15] Y. Sozer and D.A. Torrey. Modeling and control of utillity interactive inverters. *IEEE Trans. Power Electron.*, 24(11):2475–2483, Nov. 2009.

[16] L. Malesani and P. Tomasin. PWM current control techniques of voltage source converters - a survey. In *Proc. of the Int. Conf. on Ind. Electron., Control, and Inst.*, Lahaina, USA, Nov. 1993.

[17] T. Geyer. A comparison of control and modulation schemes for medium-voltage drives: emerging predictive control concepts versus field oriented control. In *Proc. IEEE Energy Conv. Congr. and Exp.*, Atlanta, USA, Sep. 2010.

[18] T. Geyer. Model predictive direct current control for multi-level converters. In *Proc. IEEE Energy Conv. Congr. and Exp.*, Atlanta, USA, Sep. 2010.